Immunity
Article

Integrin-Dependent Organization and Bidirectional Vesicular Traffic at Cytotoxic Immune Synapses

Dongfang Liu,[1] Yenan T. Bryceson,[1,2] Tobias Meckel,[1] Gaia Vasiliver-Shamis,[3] Michael L. Dustin,[3] and Eric O. Long[1,*]
[1]Laboratory of Immunogenetics, National Institute of Allergy and Infectious Diseases, National Institutes of Health, Rockville, MD 20852, USA
[2]Center for Infectious Medicine, Department of Medicine, Karolinska Institute, Karolinska University Hospital Huddinge, S-14186 Stockholm, Sweden
[3]Department of Pathology, New York University School of Medicine, and the Program in Molecular Pathogenesis, Skirball Institute of Biomolecular Medicine, 540 First Avenue, New York, NY 10016, USA
*Correspondence: elong@nih.gov
DOI 10.1016/j.immuni.2009.05.009

SUMMARY

Cytotoxic lymphocytes kill target cells by releasing the content of secretory lysosomes at the immune synapse. To understand the dynamics and control of cytotoxic immune synapses, we imaged human primary, live natural killer cells on lipid bilayers carrying ligands of activation receptors. Formation of an organized synapse was dependent on the presence of the β2 integrin ligand ICAM-1. Ligands of coactivation receptors 2B4 and NKG2D segregated into central and peripheral regions, respectively. Lysosomal protein LAMP-1 that was exocytosed during degranulation accumulated in a large and spatially stable cluster, which overlapped with a site of membrane internalization. Lysosomal compartments reached the plasma membrane at focal points adjacent to centrally accumulated LAMP-1. Imaging of fixed cells revealed that perforin-containing granules were juxtaposed to an intracellular compartment where exocytosed LAMP-1 was retrieved. Thus, cytotoxic immune synapses include a central region of bidirectional vesicular traffic, which is controlled by integrin signaling.

INTRODUCTION

Direct killing of target cells by cytotoxic T lymphocytes (CTLs) and natural killer (NK) cells contributes to immune protection from viral infections and cell transformation. CTLs and NK cells share a similar mechanism for target cell killing, which occurs through polarized release of the content of cytolytic granules (also called secretory lysosomes) toward the target cell (Orange, 2008; Stinchcombe and Griffiths, 2007). Cytotoxicity proceeds through a number of steps, including integrin-mediated adhesion to target cells, movement of cytolytic granules toward the microtubule organizing center (MTOC), and reorientation of the MTOC toward the target cell. Effector molecules in the cytotoxic pathway include perforin and members of the granzyme family of proteases, which are released upon fusion of cytolytic granules with the plasma membrane, a process also known as degranulation.

Immune synapses were originally described by postfixation imaging of T cell interactions with antigen-presenting cells (Monks et al., 1998) and by live imaging of T cell interactions with supported planar bilayers presenting ICAM-1 and MHC-peptide complexes (Grakoui et al., 1999). T cell immune synapses include a central region where T cell receptor (TCR) and CD28 accumulate and a peripheral region, which includes the β2 integrin LFA-1 (CD11a-CD18) (Dustin, 2008). The synapse includes also a focal point for TCR recycling and polarized secretion of cytokines, including interleukin-2 and interferon-γ (Das et al., 2004; Huse et al., 2006), and for delivery of secretory lysosomes toward target cells during T cell cytotoxicity (Stinchcombe and Griffiths, 2007).

Unlike T cells, which express clonally distributed antigen-specific receptors, NK cells can respond in bulk to activation signals. Therefore, it is possible to study the response of primary, unmanipulated human NK cells, isolated directly from peripheral blood. NK cells kill target cells in response to two distinct stimuli: antibody-dependent cellular cytotoxicity (ADCC) through the low-affinity Fc receptor FcγRIIIA (CD16) and natural cytotoxicity through recognition of ligands on target cells by various NK cell activation receptors (Bryceson et al., 2006; Lanier, 2005; Moretta et al., 2001). Activation of NK cell cytotoxicity requires the combination of signals for granule polarization and for degranulation. These two signals can be uncoupled in NK cells, given that engagement of LFA-1 by its ligand ICAM-1 alone is sufficient to induce granule polarization but not degranulation, whereas degranulation, but not polarization, is induced by CD16 alone (Barber et al., 2004; Bryceson et al., 2005).

Planar lipid bilayers supported on glass coverslips have been used for imaging immune synapses at high resolution (Dustin et al., 2007). However, the dynamics of vesicular traffic at cytotoxic immune synapses is still poorly defined. To investigate in real time the organization of cytotoxic immune synapses in live degranulating cells, we have inserted ligands of NK cell activation receptors into lipid bilayers and acquired live images by total internal reflection fluorescence (TIRF) microscopy. Ligands for natural cytotoxicity coactivation receptors NKG2D (CD314) and 2B4 (CD244), as well as a ligand for CD16, were used for activation of primary NK cells. The specific contribution of LFA-1 was determined by inclusion of ICAM-1 in the lipid bilayers. Our live images have revealed several properties of cytotoxic immune synapses, all of which are regulated by LFA-1. The ligands of the synergistic coactivation receptors 2B4 and NKG2D segregated into a central and a peripheral region, respectively. The lysosome-associated membrane protein 1 (LAMP-1, also known as CD107a) delivered to the cell surface

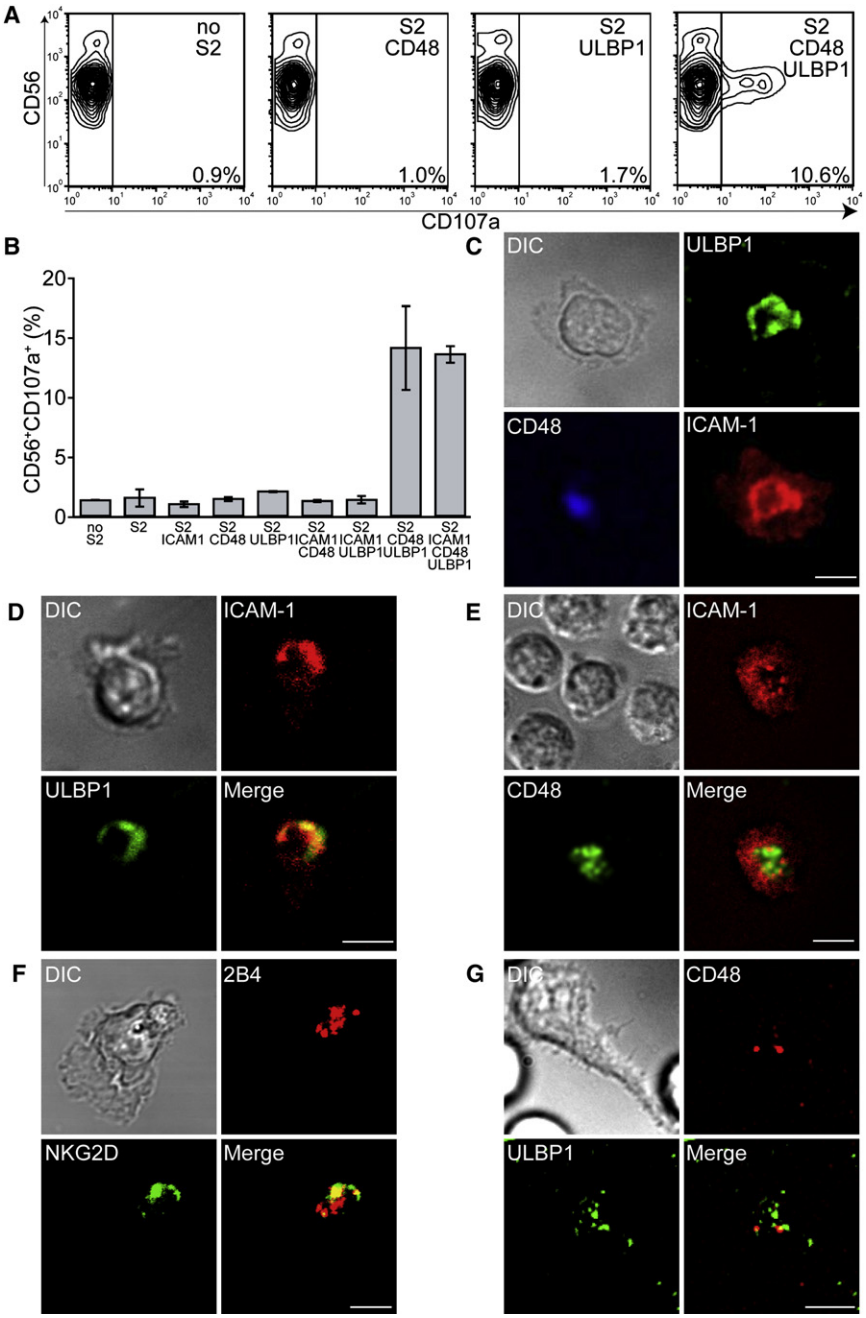

Figure 1. ICAM-1 Controls the Organization of Natural Cytotoxicity Immune Synapses

(A) CD107a staining of resting NK cells after mixing with S2 insect cells transfected with the indicated ligands. A control without S2 cells is also shown.

(B) Percentage of $CD107a^+$ NK cells after mixing with the indicated transfected S2 cells. Error bars indicate standard deviation (SD) of five independent experiments.

(C) TIRF image of an NK cell fixed 60 min after addition to a bilayer carrying ICAM-1-Alexa Fluor 568, ULBP1-Alexa Fluor 488, and CD48-Alexa Fluor 647.

(D) TIRF image of a live NK cell at ~60 min after addition to a bilayer carrying ICAM-1-Alexa Fluor 568, ULBP1-Alexa Fluor 488, and unlabeled CD48.

(E) TIRF image of live NKs cell at ~130 min after addition to a bilayer carrying ICAM-1-Alexa Fluor 568, CD48-Alexa Fluor 488, and unlabeled ULBP1.

(F) Confocal image of an NK cell fixed ~60 min after addition to a bilayer carrying unlabeled CD48 and ULBP1. Fixed and permeabilized cells were incubated with Abs to 2B4 and NKG2D and then incubated with Alexa Fluor 568- and Alexa Fluor 488-conjugated secondary Abs, respectively.

(G) TIRF image of live NK cells at ~90 min after addition to a bilayer carrying CD48-Alexa Fluor 568 and ULBP1-Alexa Fluor 488. NK cells in contact with CD48 and ULBP1 typically assumed elongated shapes. Scale bars represent 5.0 μm. The images are representative of at least 20 cells in three independent experiments.

during degranulation was contained within a central region and retrieved into an intracellular compartment. Finally, perforin-containing cytolytic granules reached the plasma membrane at focal points adjacent to accumulated LAMP-1. Thus, LFA-1 controls both the organization and vesicular traffic at cytotoxic synapses.

RESULTS

ICAM-1 Imposes a Distinct Ligand Distribution in Cytotoxic NK Cell Immune Synapses

Expression of CD48, a ligand for 2B4, or ULBP1, a ligand for NKG2D, on transfected *Drosophila* Schneider line 2 (S2) cells (Figure S1 available online) was not sufficient to induce degranulation by resting NK cells, as measured by flow cytometry with a CD107a Ab (Figure 1A). However, co-expression of CD48 and ULBP1 on S2 cells induced degranulation (Figure 1A). As shown previously (Bryceson et al., 2005), ICAM-1 did not induce degranulation (Figure 1B). Furthermore, ICAM-1 did not enhance the degranulation induced by CD48, ULBP1, or the combination of CD48 and ULBP1 (Figure 1B).

Primary human NK cells were added to planar lipid bilayers carrying ligands of the three NK cell receptors LFA-1, 2B4, and NKG2D, and the distribution of ligands was imaged by TIRF microscopy. Images of fixed NK cells revealed a characteristic distribution: CD48 accumulated predominantly in the center of the synapse, whereas ULBP1 and ICAM-1 were mainly in a region surrounding the central CD48 (Figure 1C). This organized pattern occurred in all NK cells imaged (>20 cells). When NK cells were imaged less than 30 min after injection onto lipid bilayers, 18 out of 22 imaged cells had an organized synapse (data not shown). When images were also acquired in real time, all three ligands were again included on the lipid bilayer but only two out of the three were labeled and visualized at a time, as shown with ICAM-1 and ULBP1 (Figure 1D), and ICAM-1 and CD48 (Figure 1E and Movie S1).

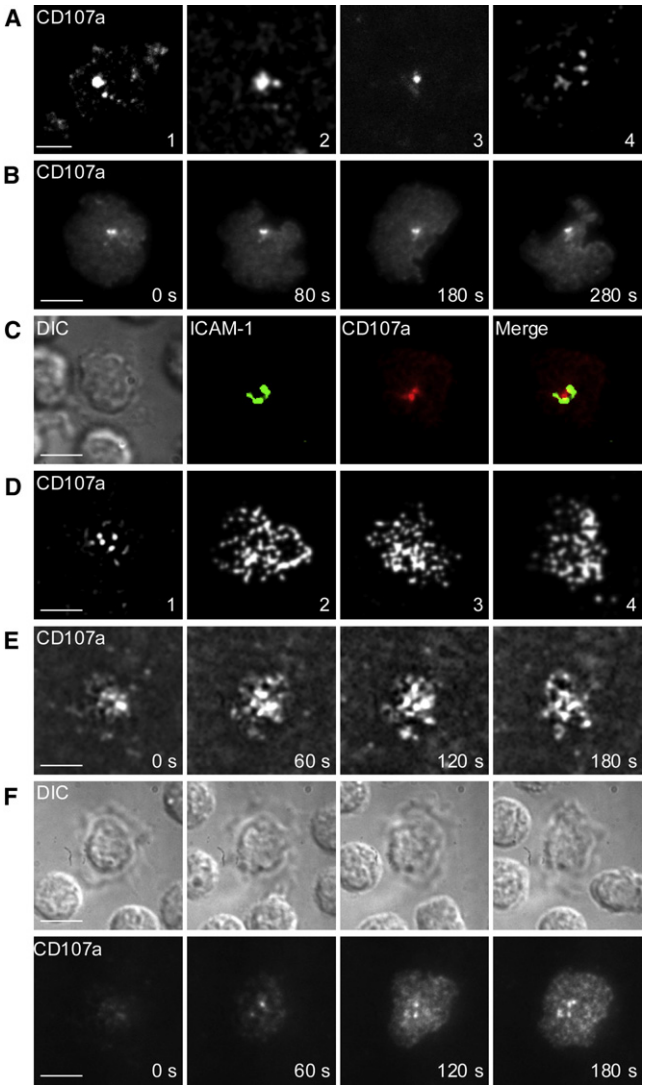

Figure 2. LAMP-1 Accumulates in a Central Cluster within Cytotoxic Immune Synapses

Degranulation was monitored by TIRF microscopy with a soluble CD107a F(ab) conjugated with Alexa Fluor 647.

(A–C) Live NK cells imaged on bilayers carrying ICAM-1, CD48, and ULBP1.

(A) Individual cells imaged at ~100 min (1), ~120 min (2), ~180 min (3), and ~60 min (4), after addition to the bilayer.

(B) Time-lapsed images taken at ~120 min after addition of NK cells to the bilayer.

(C) NK cells imaged at ~120 min after addition to a bilayer carrying unlabeled CD48 and ULBP1 and Alexa Fluor 488-conjugated ICAM-1.

(D–F) Live NK cells imaged on bilayers carrying unlabeled CD48 and ULBP1.

(D) Individual cells imaged at ~90 min (1), ~120 min (2), ~120 min (3), and ~180 min (4) after addition to the bilayer.

(E) Time-lapsed images taken at ~120 min after addition of NK cells to the bilayer.

(F) NK cells imaged ~200 min after addition to the lipid bilayer. Time-lapsed DIC (top panel) and TIRF (bottom panel) images are shown. Scale bars represent 5.0 μm. The images are representative of at least 30 cells in five independent experiments.

In agreement with images of fixed cells (Figure 1C), ICAM-1 and ULBP1 were distributed around a central region (Figure 1D), whereas CD48 remained in the center, surrounded by ICAM-1 (Figure 1E and Movie S1). The combination of CD48 and ULBP1, which is sufficient to induce degranulation (Figure 1A), resulted in the distribution of these two ligands into separate clusters, as seen in confocal images of fixed cells (Figure 1F) and in live TIRF images (Figure 1G).

To test whether a similar synapse organization would occur when NK cells contact a target cell membrane rather than a flat lipid bilayer, we imaged fixed conjugates of resting NK cells with transfected *Drosophila* S2 cells. In this case, the receptors were visualized with antibodies (Abs) to LFA-1, 2B4, and NKG2D. In conjugates with S2-ICAM-1-CD48-ULBP1 cells (Figure S1), 2B4 was distributed more centrally, surrounded by LFA-1 and NKG2D (Figure S2). The distribution of NKG2D was often diffuse rather than peripheral. In conjugates with S2-CD48-ULBP1 cells, the distribution of 2B4 and NKG2D was not concentric (Figure S2). Thus, the distribution of receptors on NK cells in contact with target cells was similar to the distribution of their ligands on lipid bilayers. Thus, coengagement of LFA-1 is required for the formation of stable, organized synapses. ICAM-1 promoted the accumulation of CD48 in a central region and partially colocalized with ULBP1 in a peripheral region.

Accumulation of LAMP-1 within a Stable Region at the Center of Cytotoxic Immune Synapses

To test whether degranulation was induced by ligands on lipid bilayers, we included a directly labeled Fab of a CD107a mAb in the lipid bilayer chamber and imaged it by TIRF microscopy, as described (Beal et al., 2008). The assay was first validated with NK cells stimulated by Phorbol 12-myristate 13-acetate (PMA) and ionomycin on a lipid bilayer carrying ICAM-1. Approximately 15 min after stimulation, NK cells acquired CD107a Fab staining (Figure S3A). Clusters of exocytosed LAMP-1 then appeared, and their distribution was dynamic and dispersed over the entire contact area with the lipid bilayer (Figure S3A). As expected for primary, resting NK cells, a sizable fraction of the NK cell population did not degranulate, which provided an internal negative control for CD107a staining (Figure S3A and S3B).

When NK cells were incubated on bilayers carrying ICAM-1, CD48, and ULBP1, a strong CD107a signal accumulated at the center of the synapse (cells 1, 2, and 3 in Figure 2A). Occasionally, several clusters of LAMP-1 were visible (cell 4 in Figure 2A). Most images were acquired 1 hr or more after addition of NK cells into the imaging chamber because of the heterogeneous time it took for primary NK cells to respond. Resting NK cells were very tentative in their decision to degranulate. Conjugation of NK cells with sensitive target cells is known to be more deliberate than that of cytotoxic T cells with specific target cells (Wulfing et al., 2003). Live imaging revealed that the site of LAMP-1 accumulation was stable over time and space and acted as an "anchor" for motile NK cells, which were protruding in several directions (Figure 2B and Movie S2). As shown by two-color live imaging, the stable site of LAMP-1 accumulation was within a ring-like distribution of ICAM-1 (Figure 2C). In contrast, on lipid bilayers carrying CD48 and ULBP1 in the absence of ICAM-1,

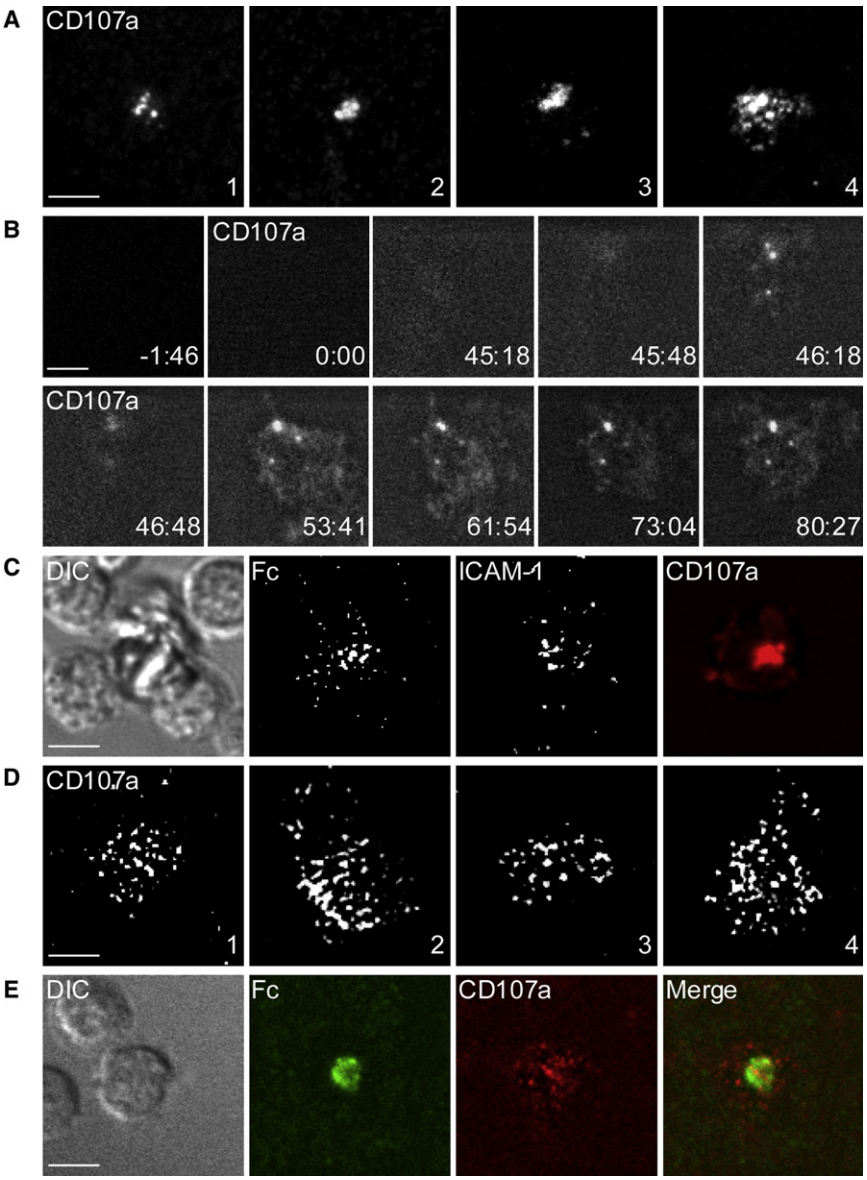

Figure 3. Central Accumulation of LAMP-1 in Synapses Formed over Ligands for LFA-1 and CD16

Degranulation was monitored by TIRF microscopy with a soluble CD107a F(ab) conjugated with Alexa Fluor 647.

(A and B) Live NK cells imaged on bilayers carrying unlabeled ICAM-1 and IgG1 Fc.

(A) Individual cells imaged at ~50 min (1), ~80 min (2), ~120 min (3), and ~26 min (4), after addition to the bilayer.

(B) Time series taken from Movie S4. The first frame was taken prior to the addition of CD107a Fab and of NK cells. The second frame was taken at the time of CD107a Fab and NK cell injection into the chamber.

(C) NK cells imaged at ~120 min after addition to a bilayer carrying Alexa Fluor 488-conjugated ICAM-1 and Alexa Fluor 568-conjugated Fc.

(D and E) Live NK cells imaged on bilayers carrying IgG1 Fc alone.

(D) Individual cells imaged at ~30 min (1), ~40 min (2), ~60 min (3), and ~100 min (4) after addition to the bilayer.

(E) NK cells imaged at ~30 min after addition to a bilayer carrying Alexa Fluor 488-conjugated Fc. Scale bars represent 5.0 μm. The images are representative of at least 50 cells in five independent experiments.

multiple clusters of LAMP-1 remained dispersed over the entire synapse, without central accumulation (Figures 2D and 2E; Movie S3). Figure 2F represents time-lapsed imaging of an NK cell in the early phase of degranulation. LAMP-1 staining increased gradually while the NK cell was spreading over the bilayer containing CD48 and ULBP1. We conclude that the accumulation and the confinement of exocytosed LAMP-1 into a stable cluster in cytotoxic synapses are regulated by LFA-1 engagement.

Central Accumulation of LAMP-1 in Synapses Formed over Ligands for LFA-1 and CD16

To compare synapses induced by coactivation receptors for natural cytotoxicity with those induced by CD16, we imaged NK cells over lipid bilayers carrying ICAM-1 and Fc of human IgG1. LAMP-1 released to the surface of degranulating NK cells accumulated in a central region (cells 1, 2, and 3 in Figure 3A), as it did on lipid bilayers carrying ligands of natural cytotoxicity receptors (Figure 2A). The central accumulation of LAMP-1 was not simply a reflection of membrane accumulation, as shown by double staining with CD107a and the membrane dye DiIC16 (Figure S4). Occasionally, the distribution of exocytosed LAMP-1 was more dispersed, but formation of a stable cluster of LAMP-1 was still apparent (cell 4 in Figure 3A). To test whether the stable LAMP-1 cluster formed through retrieval and accumulation of dispersed exocytosed LAMP-1 or whether it developed at a central point from the outset of degranulation, we initiated long-term recordings of individual cells prior to degranulation. As shown in Figure 3B and Movie S4, at the first steady appearance of exocytosed LAMP-1, a cluster that became the prominent and stable cluster had already formed. These results suggest that a central and stable region of LAMP-1 accumulation is in place early during degranulation.

Despite the formation of a stable cluster of exocytosed LAMP-1, ICAM-1 and Fc segregated in separate, disorganized, and unstable clusters (Figure 3C). This was confirmed by imaging fixed cells by confocal microscopy and by two-color live TIRF imaging (Figure S5). Thus, "ADCC synapses" formed by NK cells over ICAM-1 and IgG1 Fc on lipid bilayers did not have an organized ligand distribution.

Because degranulation by resting NK cells is also induced by CD16 signals alone (Bryceson et al., 2005), we imaged cytotoxic synapses formed over lipid bilayers carrying IgG1 Fc.

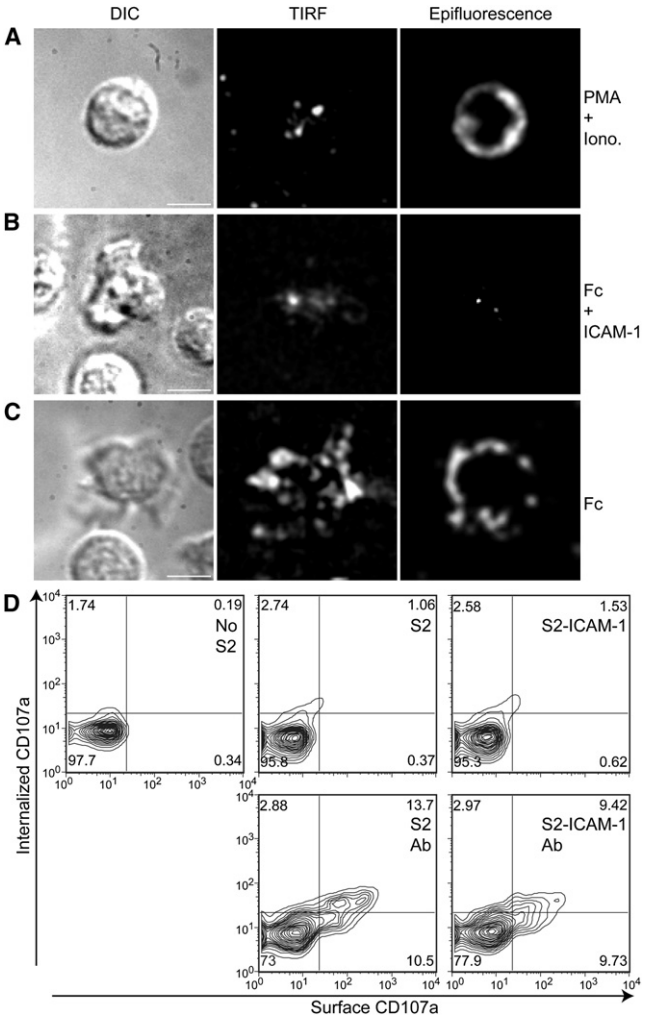

Figure 4. Diffusion of LAMP-1 on Degranulating Cells Is Constrained in the Presence of ICAM-1

(A–C) Live NK cells over lipid bilayers were imaged by DIC, TIRF, and epifluorescence, after incubation with a soluble CD107a F(ab) conjugated with Alexa Fluor 647. The DIC, TIRF, and epifluorescence images were acquired within 1 s of each other.

(A) NK cell on a bilayer carrying unlabeled ICAM-1 imaged 20 min after addition of PMA and ionomycin.

(B) NK cells imaged ~140 min after addition to a bilayer carrying unlabeled ICAM-1 and Fc.

(C) NK cells imaged ~37 min after addition to a bilayer carrying unlabeled Fc alone.

(D) Staining of extracellular and internalized LAMP-1 with CD107a Ab 2 hr after mixing NK cells with S2 cells, S2 cells transfected with ICAM-1, and S2 cells coated with rabbit antiserum (Ab), as indicated. NK cells were gated by staining with FITC-conjugated CD56 mAb. Selective staining of internalized LAMP-1 by PE and of cell surface LAMP-1 by allophycocyanin with biotinylated CD107a Ab is described in the Experimental Procedures. Scale bars represent 5.0 μm. The images are representative of ten cells in three independent experiments.

Exocytosed LAMP-1 appeared in multiple dispersed clusters (Figure 3D). The pattern of dispersed LAMP-1 clusters was observed at the very first appearance of exocytosed LAMP-1 at the beginning of degranulation. Occasionally, more extensive clustering of LAMP-1 was observed (Movie S5), particularly at a higher density of Fc (400–500 molecules/μm^2). However, these large LAMP-1 clusters were not spatially and temporally stable (Movie S5), in contrast to the stable clusters formed in the presence of ICAM-1 and Fc. Two-color live imaging revealed that LAMP-1 clusters remained dispersed even when Fc clustered at the center of the synapse (Figure 3E). NK cells injected over lipid bilayers carrying Fc alone not only degranulated but also promoted rapid and stable clustering of Fc (Figure 3E; Figure S6). In conclusion, ICAM-1 promoted accumulation of LAMP-1 in a stable cluster after activation of NK cell degranulation by CD16 as well as natural cytotoxicity receptors.

LFA-1 Prevents Diffusion of Exocytosed LAMP-1 and Promotes LAMP-1 Retrieval in a Central Region

We evaluated diffusion and retrieval of exocytosed LAMP-1 by combining images taken by TIRF and epifluorescence microscopy, within 1 s of each other. If LAMP-1 were free to diffuse at the surface of degranulating cells, it should be visible as a ring under epifluorescence. To test it, we imaged NK cells stimulated by PMA and ionomycin over bilayers carrying ICAM-1. As expected for the receptor-independent degranulation induced by PMA and ionomycin, LAMP-1 was detected in multiple clusters under TIRF and at the cell periphery under epifluorescence (Figure 4A). Note that the peripheral distribution of LAMP-1 may include molecules at the cell surface and molecules that have been retrieved by internalization. These results show that receptor-independent degranulation did not lead to accumulation of exocytosed LAMP-1 in a specific region of the cell. In contrast, NK cells that degranulated in response to CD16 in the presence of ICAM-1 retained exocytosed LAMP-1 close to the site of contact, as shown by the lack of staining of the cell periphery under epifluorescence and by the presence of a central LAMP-1 cluster under TIRF imaging (Figure 4B). Finally, the distribution of LAMP-1 on NK cells that degranulated over lipid bilayers carrying Fc alone was similar to that obtained after stimulation with PMA and ionomycin and showed that LAMP-1 was not retained within the synapse (Figure 4C). Therefore, engagement of LFA-1 promotes polarized degranulation and prevents the diffusion of exocytosed LAMP-1 around the cell periphery.

We used an assay developed to measure simultaneously exocytosed LAMP-1 at the cell surface and exocytosed LAMP-1 that has been retrieved into the cell (Bryceson et al., 2005) to monitor degranulation and LAMP-1 internalization in the presence or absence of ICAM-1 on S2 insect cells. Activation through CD16 by a rabbit anti-S2 cell serum stimulated exocytosis of LAMP-1 and LAMP-1 internalization (Figure 4D). The diagonal two-color staining for surface and for internalized LAMP-1 indicated that internalization was proportional to LAMP-1 exocytosis. The same balance between LAMP-1 exocytosis and internalization was observed during activation through CD16 in the presence of ICAM-1 (Figure 4D). Therefore, the major control exerted by ICAM-1 on the distribution of exocytosed LAMP-1 and its retrieval into a stable cluster was not due to major changes in the rate of LAMP-1 exocytosis and internalization. Our data supports the conclusion that engagement of LFA-1 by ICAM-1 prevents the diffusion of exocytosed LAMP-1 and promotes its accumulation in a central region of the synapse.

A quantitative analysis was performed by single-molecule imaging of CD107a Fab. To relate the fluorescence intensity to

the number of Fab molecules, we quantified the intensity of single Fab particle signals and of Fab clusters in the same recordings. CD107a Fab was loaded over the lipid bilayer at different concentrations in the absence of NK cells. Intensities of the diffraction-limited spots had the same distribution, regardless of the concentration of the Fab solution (Figure S7). Such a dilution-independent intensity is only possible for single molecules. The full width at half-maximum (FWHM) was measured as an indicator of the single structure size. Each single Fab followed a Gaussian distribution with a FWHM of 435 ± 17 nm for Alexa Fluor-647, suggesting an imaging resolution of ~435 nm (Figure S8). This quantitative analytical approach was applied so that the number of CD107a Fab molecules per cluster could be determined. Most clusters of exocytosed LAMP-1 formed in the absence of ICAM-1 carried a few Fab molecules (11.2 ± 1.7 for CD48+ULBP1, n = 26, and 10.4 ± 1.1 for Fc, n = 27), similar to clusters obtained by stimulation with PMA and ionomycin (8.9 ± 2.1 Fab molecules, n = 28) (Figure S9). Ten out of 36 clusters induced by CD48 and ULBP1 had 106.8 ± 17.5 Fab molecules, and 2 out 29 induced by Fc had ~55 Fab molecules (Figure S9). However, these larger LAMP-1 clusters formed in the absence of ICAM-1 were neither spatially nor temporally stable (Movie S5). Addition of ICAM-1 on the bilayer caused a major shift in the number of Fab molecules bound per cluster: namely 214.7 ± 37.5 (n = 15) for CD48, ULBP1, and ICAM-1 and 212.7 ± 39.2 (n = 17) for Fc with ICAM-1 (Figure S9). Therefore, the presence of ICAM-1 on the lipid bilayer resulted in accumulation of ~20 times more exocytosed LAMP-1 molecules per cluster.

Active Membrane Internalization at the Site of LAMP-1 Accumulation

The stable cluster of LAMP-1 formed in the presence of ICAM-1 may represent accumulation at the cell surface of LAMP-1 molecules that have been exocytosed. However, the recycling of exocytosed LAMP-1 to intracellular compartments in degranulating cells (Figure 4D) suggested that the central accumulation of LAMP-1 might also correspond to a site of internalization. To visualize membrane internalization in live NK cells, we used the membrane-impermeable FM1-43 styryl dye to label the plasma membrane. FM1-43 inserts into but does not traverse membranes because of its hydrophilic head (Cousin, 2008). FM1-43 therefore labels the plasma membrane and membranes that have been internalized from the cell surface. FM1-43 can be removed from solvent-accessible membranes by the sulfobutylated derivative of β-cyclodextrin ADVASEP-7 (Kay et al., 1999). To validate this system, we labeled NK cells and the lipid bilayer separately with FM1-43 (Figure S10A and S10B). A "destain" with ADVASEP-7 greatly reduced the fluorescence signal (Figures S10A and S10B). To test whether membrane internalization could be observed in live NK cells by this technique, we stimulated NK cells labeled with FM1-43 with PMA and ionomycin and destained them with ADVASEP-7. FM1-43 labeling at the cell periphery was clearly observed before destaining (Figure S10C), whereas internalized membranes visible as distinct vesicles were detected after destaining with ADVASEP-7 (Figure S10C).

We used the FM1-43 stain-stimulate-destain protocol outlined in Figure 5A to visualize membrane internalization in NK cells stimulated on lipid bilayers. NK cells that degranulated in response to PMA and ionomycin showed membrane internalization in multiple compartments, which did not overlap with LAMP-1 clusters (Figure 5B). In live images, both FM1-43-labeled vesicles and LAMP-1 clusters were highly dynamic (data not shown). Stimulation by CD48 and ULBP1 in the presence of ICAM-1 resulted in strong membrane internalization at a site that overlapped with centrally accumulated LAMP-1 (Figure 5C and Movie S6). In contrast, CD48 and ULBP1 in the absence of ICAM-1 induced membrane internalization at multiple, mobile, and dispersed sites, which did not colocalize with clusters of exocytosed LAMP-1 (Figure 5D). Therefore, ICAM-1 promoted the formation of a central region where LAMP-1 accumulated and where membrane was actively internalized. This was also observed after stimulation by Fc and ICAM-1, given that a strong FM1-43 signal from internalized membrane overlapped with centrally accumulated LAMP-1 (Figure 5E and Movie S7). The fluorescence intensity of accumulated LAMP-1 and of internalized FM1-43 showed fluctuations over time, indicating dynamic processes. Segregation of internalized FM1-43 and exocytosed LAMP-1 into separate and multiple clusters was observed in NK cells stimulated by Fc alone (Figure 5F), similar to results obtained with NK cells on CD48 and ULBP1 (Figure 5D). Colocalization of internalized FM1-43 and accumulated LAMP-1 was analyzed quantitatively. The Pearson correlation coefficient (γ) was 0.29 and 0.28 in the absence of ICAM-1 (Figures 5D and 5F, respectively) and 0.85 and 0.90 in the presence of ICAM-1 (Figures 5C and 5E, respectively). These data clearly show that the accumulation of LAMP-1 in a stable cluster on NK cells that degranulate in the presence of ICAM-1 corresponds to a site of active membrane internalization.

Lysosomal Compartments Contact the Plasma Membrane at Focal Points Adjacent to Accumulated LAMP-1

The critical role of LFA-1 in promoting granule polarization, organization of NK cell cytotoxic immune synapses, and formation of a region of membrane internalization where LAMP-1 accumulates suggested that LFA-1 might also control the point at which secretory lysosomes reach the plasma membrane during NK cell degranulation. To test this possibility, we labeled lysosomal compartments in primary, live NK cells with LysoTracker Green DND-26. The pH of lytic granules in NK cells is ~4.8 (Liu et al., 2005). The evanescent field, in which the sample is illuminated during TIRF microscopy, is shorter than 200 nm (its calculated value was 87 nm) and decays exponentially with distance from the slide. It is therefore narrower than the diameter of a single lytic granule, which is ~400 nm (Burkhardt et al., 1993; Stinchcombe et al., 2001). Therefore, cytolytic granules visible as LysoTracker-positive compartments by TIRF microscopy would have to be "docked" at, or be very close to the plasma membrane. LysoTracker-loaded NK cells on poly-lysine-coated slides revealed multiple vesicles, some of which moved laterally along the plasma membrane while others moved into and out of the evanescent field (Figure S11 and Movie S8).

A different picture emerged when lysosomal compartments were imaged in NK cells that degranulated in the presence of ICAM-1. Stimulation by CD48 and ULPB1 induced appearance of lysosomal compartments that remained in close proximity to the stable cluster of LAMP-1 (Figures 6A and 6B, Movie S9). In

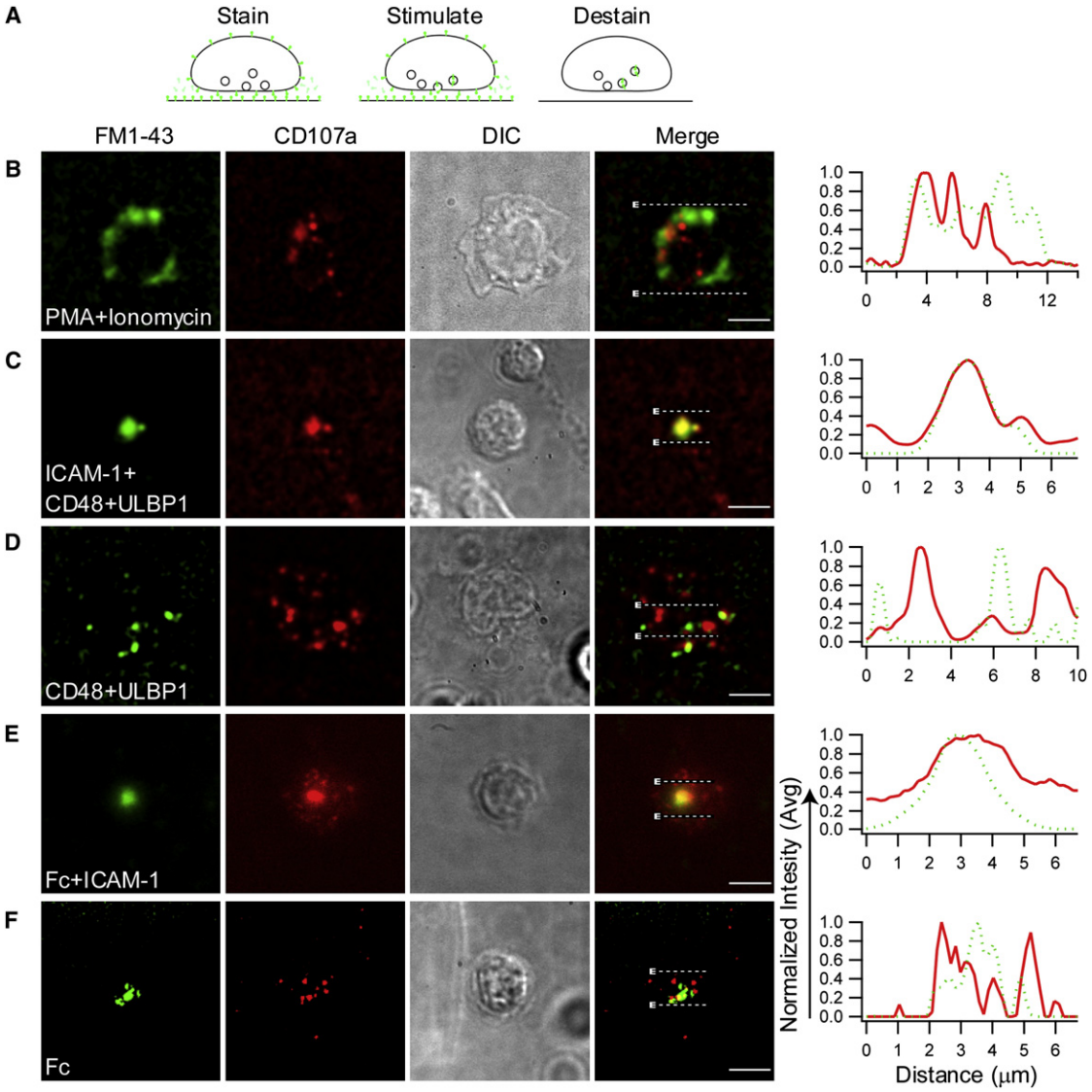

Figure 5. Internalized Membranes Colocalize with Centrally Accumulated LAMP-1

(A) Internalized membranes in FM1-43-labeled and stimulated NK cells were detected by TIRF microscopy after destaining with ADVASEP-7. FM1-43 has almost no fluorescent properties in aqueous solution. NK cells were incubated with 8.0 μM FM1-43 at 37°C for 5 min and injected into Bioptechs chamber for 60 min. For destaining, FM1-43 was stripped for 2 min with 1.0 mM ADVASEP-7.

(B–F) Degranulation was monitored by TIRF microscopy with a soluble CD107a F(ab) conjugated with Alexa Fluor 647. The DIC, FM1-43, and LAMP-1 images were acquired within 1 s of each other. The normalized intensity of CD107a (red lines) and FM1-43 (green lines) signals within the parallel horizons indicated in the composites were graphed in the right panels.

(B) PMA and ionomycin-stimulated NK cells imaged ~20 min after addition to a bilayer carrying unlabeled ICAM-1.

(C) NK cells imaged ~160 min after addition to a bilayer carrying unlabeled CD48, ULBP1, and ICAM-1.

(D) NK cells imaged ~200 min after addition to a bilayer carrying unlabeled CD48 and ULBP1.

(E) NK cells imaged ~120 min after addition to a bilayer carrying unlabeled Fc and ICAM-1.

(F) NK cells imaged ~60 min after addition to a bilayer carrying unlabeled Fc. Scale bars represent 5.0 μm. The images are representative of at least 20 cells in three independent experiments.

the absence of ICAM-1, contacts of lysosomal compartments with the plasma membrane were mobile, dispersed, and not concentrated around LAMP-1 clusters (Figures 6C and 6D; Movie S10). In NK cells stimulated by Fc and ICAM-1, lysosomal compartments were again adjacent to the stable LAMP-1 clusters (Figure 6E, Movie S11, and Figure S12). In an NK cell that had two LAMP-1 clusters, each one was stably paired with a lysosomal compartment (Figure 6F and Movie S12). In the absence of ICAM-1, membrane-proximal lysosomal compartments and LAMP-1 clusters were mobile and dispersed over a large area of the cytotoxic synapse (Figures 6G and 6H). The lateral mobility of objects can be rendered in 2D by a "time projection," which is in effect a z stack projection where z = time. Time projections for NK cells stimulated by each of the

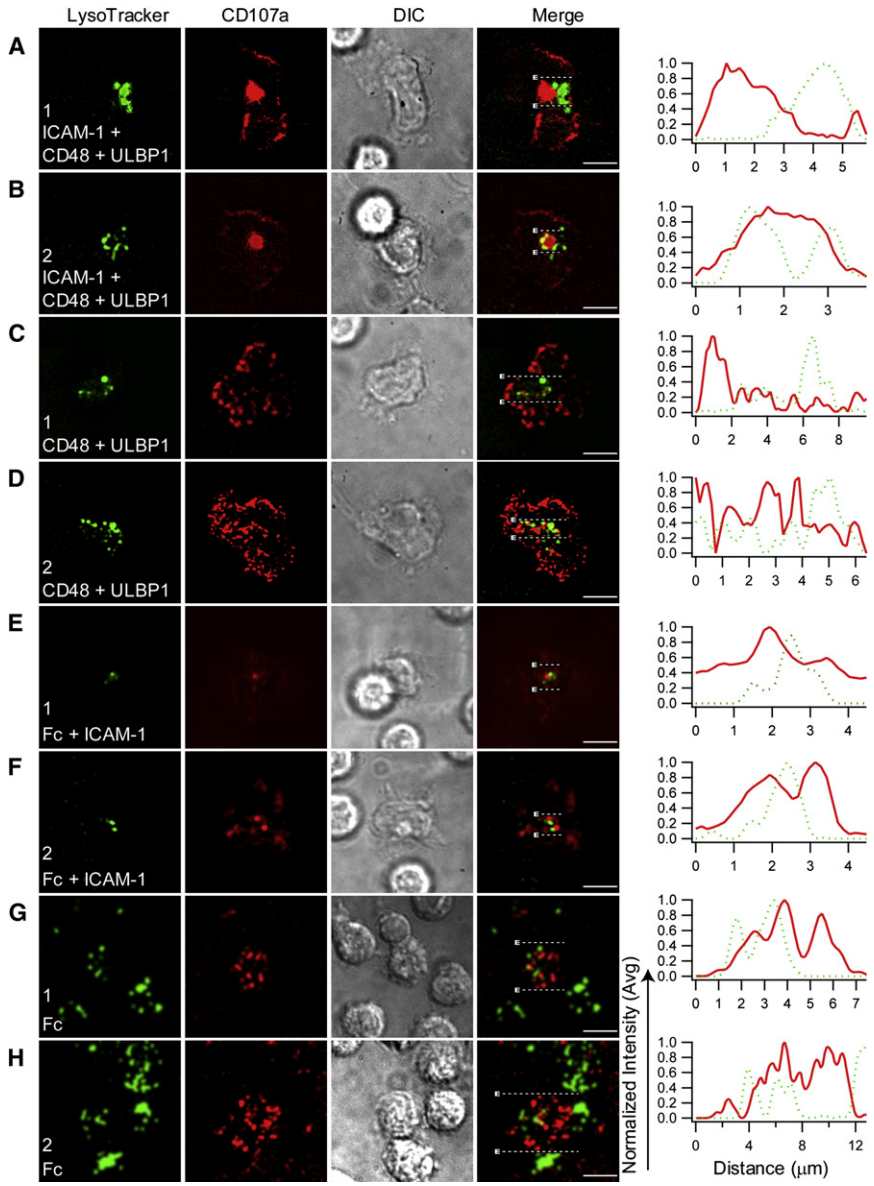

Figure 6. Lysosomal Compartments Reach the Plasma Membrane at Focal Points Adjacent to Accumulated LAMP-1

Lysosomal compartments labeled with LysoTracker Green and exocytosed LAMP-1 labeled with a soluble CD107a Fab conjugated with Alexa Fluor 647 were imaged by TIRF microscopy. DIC and TIRF images were acquired within 1 s of each other. The normalized intensity of CD107a (red lines) and LysoTracker (green lines) over the parallel horizon indicated in the merged images are shown in the panels on the right.

(A and B) NK cells imaged on bilayers carrying unlabeled CD48, ULBP1, and ICAM-1 ~90 min (1) and ~170 min (2) after injection over the bilayer.

(C and D) NK cells imaged on bilayers carrying unlabeled CD48 and ULBP1 ~88 min (1) and ~260 min (2) after injection over the bilayer.

(E and F) NK cells imaged on bilayers carrying unlabeled Fc and ICAM-1 ~130 min (1) and ~50 min (2) after injection over the bilayer.

(G and H) NK cells imaged on bilayers carrying unlabeled Fc ~60 min (1) and ~130 min (2) after injection over the bilayer. Scale bars represent 5.0 μm. The images are representative of at least 50 cells in three independent experiments.

four ligand combinations illustrated how lysosomal compartments at the plasma membrane remained juxtaposed to accumulated LAMP-1 in the presence of ICAM-1 (Figure S13). Kymographs, which depict changes in intensity over time for a given slice through a 2D image, also illustrated the ICAM-1-dependent stability of adjacent LAMP-1 clusters and lysosomal compartments at the plasma membrane (Figure S14). These results demonstrated that ICAM-1 promoted the formation of focal points in cytotoxic immune synapses where lysosomal compartments reached the plasma membrane and where exocytosed LAMP-1 accumulated.

Perforin-Containing Granules Are Adjacent to Internalized LAMP-1

Three-dimensional imaging of fixed cells was performed to address two main questions: are the stable LAMP-1 clusters intracellular, and are the adjacent lysosomal compartments cytolytic granules? Resting NK cells incubated in the presence of a CD107a Fab on lipid bilayers carrying ICAM-1 and Fc were fixed and stained with Abs to perforin and tubulin. The stable clusters of LAMP-1 were in large intracellular vesicles (Figure 7A), consistent with data correlating LAMP-1 exocytosis with endocytosis (Figure 4D) and data showing colocalization with internalized membrane (Figures 5C and 5E). Furthermore, perforin-containing granules were juxtaposed to internalized LAMP-1 (Figure 7A), strongly suggesting that lysosomal compartments adjacent to LAMP-1 clusters near the plasma membrane in live cells (Figure 6) were cytolytic granules. Finally, as expected, the MTOC was oriented toward the synapse (Figure 7A). A rotating 3D view clearly shows that the LAMP-1 compartment and the cytolytic granules are in close proximity to each other and to the lipid bilayer and that the MTOC is oriented toward the synapse (Movie S13). In the absence of ICAM-1, LAMP-1 clusters were faint and dispersed, and neither perforin-containing granules nor MTOC were polarized toward the synapse (Figure 7B and Movie S14). ICAM-1-dependent polarization of granules and MTOC was also observed in NK cells conjugated with *Drosophila* S2 cells (Figure S15).

To test whether the same LFA-1-dependent distribution of exocytosed LAMP-1 and of cytolytic granules occurred when NK cells were in contact with target cells during natural cytotoxicity, we fixed NK cells incubated with S2-ICAM-1-CD48-ULBP1 insect cells in the presence of the CD107a Fab and imaged them by 3D confocal microscopy. One or two clusters of LAMP-1 were

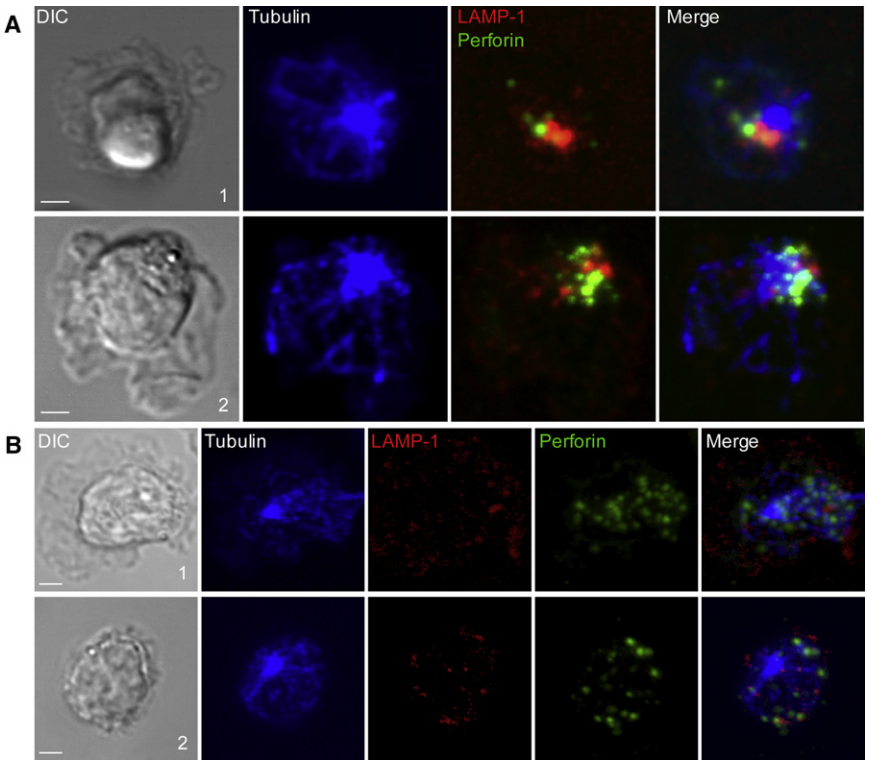

Figure 7. Polarized Perforin-Containing Lytic Granules Contact Internalized LAMP-1 in the Presence of ICAM-1

(A) NK cells imaged on bilayers containing Fc and ICAM-1 ~60 min (1) and ~120 min (2) after injection over the bilayer. Perforin (green), internalized LAMP-1 (red), and Tubulin (blue) were acquired by 3D confocal microscopy. Scale bars represent 5.0 μm. The images are representative of at least 30 cells in two independent experiments.

(B) NK cells imaged on bilayers carrying Fc ~120 min after injection over bilayer. Scale bars represent 2.0 μm. The images are representative of 50 cells in three independent experiments. Differential interference contrast (DIC) images are shown on the left. Merged overlays of fluorescence are on the right. LAMP-1 was detected by inclusion of 0.016 μM Alexa Fluor 647-labeled CD107a Fab during NK cell incubation on with lipid bilayer containing Fc.

observed at or near the cell surface, and each LAMP-1 cluster was juxtaposed to a perforin-containing granule (Figure S16). Granule polarization was not observed in NK cells conjugated with S2-CD48-ULBP1 cells. We conclude that cytotoxic immune synapses include an LFA-1-dependent, stable zone where cytolytic granules polarize to fuse with the plasma membrane and a separate endocytic compartment where LAMP-1 that has been exocytosed during degranulation is retrieved into the cell.

DISCUSSION

Cellular cytotoxicity by T cells and NK cells, a process through which infected or transformed cells are eliminated, is regulated through the formation of stable immunological synapses. In this study, we provided dynamic, high-resolution images of cytotoxic immune synapses formed over lipid bilayers carrying ligands of NK cell activation receptors. Degranulating cells were identified and visualized through appearance of LAMP-1 at the cell surface (Beal et al., 2008). The organization of NK cell cytotoxic immune synapses required the LFA-1 ligand ICAM-1, which promoted segregation of ligands for the synergistic coactivation receptors 2B4 and NKG2D into a central and peripheral region, respectively. A similar organization was observed for the receptors on NK cells during contact with insect cells expressing ligands of human NK cell receptors. ICAM-1 promoted not only spatial organization of receptor-ligand distribution but also the formation of a central zone in the synapse with unique properties. LAMP-1 exocytosed during degranulation did not escape and diffuse over the plasma membrane but accumulated in a stable, central cluster in which membrane internalization occurred. Furthermore, the central region included focal points for the contact of lysosomal compartments with the plasma membrane, which were directly adjacent to accumulated LAMP-1. Three-dimensional reconstructions of cells fixed after degranulation established that perforin-containing granules were in close proximity to a large intracellular compartment containing LAMP-1 recycled from the surface. These results, obtained with primary and unmanipulated NK cells isolated directly from human peripheral blood without exogenous stimuli, revealed that the center of cytotoxic immune synapses is spatially stable and functionally dynamic because it includes zones of active internalization and exocytosis.

The distribution of receptor-ligand combinations at cytotoxic NK cell immune synapses has unique features. On lipid bilayers, ICAM-1 was distributed preferentially around a central region, similar to its distribution at T cell immune synapses, but the ligands for the synergistic coactivation receptors NKG2D and 2B4 segregated into a peripheral and a central region, respectively. The segregation of synergistic receptors NKG2D and 2B4 at NK cell immune synapses is reminiscent of the dynamic segregation of the synergistic pairs of TCR and CD28, and of TCR and CD2, at T cell immune synapses (Kaizuka et al., 2009; Yokosuka et al., 2008). Clustering of 2B4 in a central zone was observed at synapses of transfected NK cells with sensitive target cells (Roda-Navarro et al., 2004). In contrast, the related receptor CD2 segregated to a peripheral region of NK cell immune synapses (Orange et al., 2003). In other studies using lipid bilayers, mouse CD48 segregated in a zone between the central MHC and ICAM-1 at synapses of mouse T cells over ICAM-1, MHC-peptide, and CD48 (Grakoui et al., 1999). (Note that mouse CD48 binds to both 2B4 and CD2 receptors.) Mouse NK cells on a lipid bilayer carrying ICAM-1 and the NKG2D ligand Rae1 formed a synapse with Rae1 in the center and ICAM-1 in a peripheral ring (Giurisato et al., 2007). A comparison with human resting NK cells triggered by LFA-1 and NKG2D was not possible because human NK cells crawled actively over

bilayers carrying ICAM-1 and ULBP1 (data not shown). The unique, ICAM-1-dependent ligand distribution at human NK cell cytotoxic immune synapses was confirmed with NK cells in contact with insect cells, in which 2B4 was preferentially in the center, whereas NKG2D and LFA-1 were peripheral. Our results have revealed an essential role of ICAM-1 in promoting an organized distribution of receptor-ligand pairs at NK cell immune synapses.

The ADCC synapses of NK cells, which involve coengagement of CD16 and LFA-1, were not organized because Fc accumulated in multiple dynamic clusters, which overlapped only partially with ICAM-1 clusters. Yet, coengagement of CD16 and LFA-1 by their respective ligands on S2 insect cells promoted polarized degranulation and efficient killing (Bryceson et al., 2005). Despite the lack of a discernible receptor-ligand organization, NK cells formed stable ADCC synapses over ICAM-1 and Fc, which were notable for a central region of active LAMP-1 exocytosis and membrane internalization. Therefore, target cell killing by NK cell-mediated ADCC may be quite different from killing by cytotoxic T cells, in which LFA-1 and maintenance of an intact p-SMAC may be important for efficient granule-mediated killing by CTL (Anikeeva et al., 2005; Beal et al., 2008; Somersalo et al., 2004).

A striking feature of NK cell cytotoxic immune synapses formed in the presence of ICAM-1 is that LAMP-1 delivered to the cell surface did not escape and diffuse over the plasma membrane. Instead, LAMP-1 accumulated in a large and stable cluster. Imaging of NK cells at the earliest stages of degranulation suggested that ICAM-1 promotes LAMP-1 exocytosis at the center of the synapse, rather than LAMP-1 retrieval from the periphery. In support of this, ICAM-1 did not prevent LAMP-1 diffusion during receptor-independent stimulation of degranulation. During degranulation induced in the absence of ICAM-1, exocytosed LAMP-1 was distributed over the periphery of the entire cell but remained in microclusters, which would be consistent with a release of cytolytic granule content through partial fusion, without free lateral diffusion of proteins from the granule membrane. By comparison, the large clusters of LAMP-1 obtained in the presence of ICAM-1 contained, on average, 20 times more LAMP-1 molecules than these LAMP-1 microclusters.

Live imaging of membranes internalized from the cell surface in the presence of ICAM-1 on the bilayers revealed a central zone of active membrane internalization at the site of LAMP-1 accumulation. Stimulation of NK cells in the absence of ICAM-1 resulted in the distribution of internalized membrane at multiple sites, which did not correspond to microclusters of exocytosed LAMP-1. Quantitative degranulation assays with resting NK cells stimulated by S2 insect cells showed that the overall balance of LAMP-1 exocytosis and reinternalization was similar in the presence or the absence of ICAM-1. These results suggest that LFA-1 is not controlling the balance of LAMP-1 exocytosis and reinternalization directly, but prevents LAMP-1 diffusion and promotes accumulation of exocytosed LAMP-1 in a stable and central region of the synapse. Retrieval of LAMP-1 by endocytosis into a central compartment, rather than multiple sites around the cell periphery, could facilitate recycling of lysosomal membranes.

Lytic granules tethered to the plasma membrane have been observed by TIRF microscopy in the NK cell line NK92 (Liu et al., 2005). In the absence of ICAM-1, contacts of lysosomal compartments with the plasma membrane of resting NK cells occurred at multiple points within the synapse, which were not stable and not spatially related to microclusters of exocytosed LAMP-1. In contrast, in NK cells stimulated in the presence of ICAM-1 on lipid bilayers, LysoTracker-positive compartments formed stable contacts with the plasma membrane at focal points, which were tightly juxtaposed to centrally accumulated LAMP-1. As shown by imaging of fixed cells after stimulation by ligands on lipid bilayers and on insect cells, the large intracellular compartment of recycled LAMP-1 is close to perforin-containing granules.

High-resolution imaging of live and fixed cytotoxic immune synapses has revealed a stable and central zone of bidirectional traffic where cytolytic granules reach the plasma membrane and where lysosomal membranes, as defined by a high density of LAMP-1 molecules, are retrieved into the cell. This stable region of membrane dynamics is the defining feature of cytotoxic synapses, given that it occurred even without an organized distribution of LFA-1 and CD16. Our data so far suggest that traffic proceeds on a divided highway, with little exchange between outgoing and incoming vesicles, although mixing between opposing lanes, as in a two-way street, is likely to occur at some point. The identification of spatially regulated membrane dynamics at the center of NK cell immune synapses induced by two different types of activation signals suggests that it is a general feature of cytolytic immune synapses, including those of CTLs.

EXPERIMENTAL PROCEDURES

Cells

NK cells were isolated from human peripheral blood by negative selection with an NK isolation kit (Miltenyi Biotec, Auburn, CA), and were > 99% $CD3^-CD56^+$. Freshly isolated NK cells were resuspended in Iscove's modified Dulbecco medium (IMDM; Invitrogen, Carlsbad, CA) supplemented with 10% human serum (Valley Biomedical, Winchester, VA) without IL-2, and were used within 2 days.

Antibodies and Reagents

Abs and their source were as follows: 2B4 (clone 2-69, BD Biosciences); NKG2D (clone 149810, R&D Systems); CD107a purified from ascites (clone H4A3, Developmental Studies Hybridoma Bank, University of Iowa, Iowa City, IA); biotinylated CD107a Ab (clone H4A3, BD Bioscience); CD56 mAb (clone NCAM16.2, BD Bioscience); β-tubulin (clone tub2.1, Cy3-conjugated; Sigma-Aldrich); perforin mAb (δG9, Pierce Chemical Co.); CD11a (clone HI111, BD Bioscience); and Alexa Fluor 488-, 568-, and 647-labeled isotype-specific goat anti-mouse Abs (Molecular Probes). Phorbol 12-myristate 13-acetate (PMA) and ionomycin calcium salt were from Sigma-Aldrich. The 1, 2-Dioleoyl-sn-Glycero-3-Phosphocholine (DOPC) and 1, 2-Dioleoyl-sn-Glycero-3-[(N-(5-amino-1-carboxypentyl) iminodiacetic acid) succinyl] (nickel salt) (DOGS-NTA) were from Avanti Polar Lipids. The acidotropic dye LysoTracker Green DND-26 and membrane dye DiIC16 were from Molecular Probes. A 5 mM solution of DiIC16 was made in ethanol and stored at −80°C under argon. Human ICAM-1, CD48, ULBP1, and IgG1 Fc were engineered as soluble molecules fused to a 6-histidine amino acid tag and purified from the supernatants of transfected 293T cells over ProBond Nickel-chelating Resin (Invitrogen). Each protein was further purified by size-exclusion HPLC. Purified His-tagged proteins were labeled with different Alexa Fluor dyes with a protein-labeling kit (Molecular Probles). CD107a mAb was purified from ascites by Protein A-resin column (Pierce). The Fab fragment was prepared with the Immunopure Fab kit (Pierce), conjugated with Alexa Fluor 647, and further purified by Sephacryl S-200 size-exclusion HPLC (Figure S7A).

NK Cell Assays

Stimulation with PMA and ionomycin was in 100 nM and 10 μM, respectively. Staining of cell surface and internalized LAMP-1 with CD107a Ab was as described (Bryceson et al., 2005). LysoTracker Green DND-26 was diluted to 50 nM for labeling of lysosomal compartments prior to imaging by TIRF microscopy. A total of 10×10^6 NK cells in 300 μl imaging buffer (HEPES-buffered saline) were injected into FCS2 chambers containing lipid bilayers. Most of the live images were acquired once degranulating NK cells could be identified by the appearance of CD107a under TIRF microscopy. Because experiments were carried out exclusively with primary, resting NK cells, the time delay between injection into the chamber and detectable degranulation varied considerably among cells and between experimental conditions. The time delays according to stimulation conditions were increasingly longer in the following order: PMA and ionomycin, CD16, and NKG2D and 2B4 coengagement.

Membrane Internalization Assay with FM1-43

Ten million NK cells were washed twice with PBS, incubated at 37°C for 5 min with 8.0 μM FM1-43 in 300 μl imaging buffer (HEPES-buffered saline) containing 0.016 μM Alexa Fluor 647-labeled CD107a Fab, and injected into Bioptechs parallel plate flow chamber-FCS2. For destaining after NK cell activation on lipid bilayers, solvent-accessible FM1-43 was gently stripped for 2 min with 1.0 mM ADVASEP-7 in the imaging buffer with 0.016 μM Alexa Fluor 647-labeled CD107a Fab.

SUPPLEMENTAL DATA

Supplemental Data include Supplemental Experimental Procedures, 16 figures, and 14 movies and can be found with this article online at http://www.cell.com/immunity/supplemental/S1074-7613(09)00275-1.

ACKNOWLEDGMENTS

We thank T. Starr, A. Beal, Y. Sykulev, M. March, S. Radaev, J. Brzostowski, and P. Tolar for advice and help. This work has been supported by the Intramural Research Program of the National Institutes of Health, National Institute of Allergy and Infectious Diseases.

Received: December 31, 2008
Revised: April 27, 2009
Accepted: May 12, 2009
Published online: July 9, 2009

REFERENCES

Anikeeva, N., Somersalo, K., Sims, T.N., Thomas, V.K., Dustin, M.L., and Sykulev, Y. (2005). Distinct role of lymphocyte function-associated antigen-1 in mediating effective cytolytic activity by cytotoxic T lymphocytes. Proc. Natl. Acad. Sci. USA *102*, 6437–6442.

Barber, D.F., Faure, M., and Long, E.O. (2004). LFA-1 contributes an early signal for NK cell cytotoxicity. J. Immunol. *173*, 3653–3659.

Beal, A.M., Anikeeva, N., Varma, R., Cameron, T.O., Norris, P.J., Dustin, M.L., and Sykulev, Y. (2008). Protein kinase Ctheta regulates stability of the peripheral adhesion ring junction and contributes to the sensitivity of target cell lysis by CTL. J. Immunol. *181*, 4815–4824.

Bryceson, Y.T., March, M.E., Barber, D.F., Ljunggren, H.G., and Long, E.O. (2005). Cytolytic granule polarization and degranulation controlled by different receptors in resting NK cells. J. Exp. Med. *202*, 1001–1012.

Bryceson, Y.T., March, M.E., Ljunggren, H.G., and Long, E.O. (2006). Activation, coactivation, and costimulation of resting human natural killer cells. Immunol. Rev. *214*, 73–91.

Burkhardt, J.K., McIlvain, J.M., Jr., Sheetz, M.P., and Argon, Y. (1993). Lytic granules from cytotoxic T cells exhibit kinesin-dependent motility on microtubules in vitro. J. Cell Sci. *104*, 151–162.

Cousin, M.A. (2008). Use of FM1–43 and other derivatives to investigate neuronal function. Curr. Protoc. Neurosci. *Chapter 2*, Unit 2.6.

Das, V., Nal, B., Dujeancourt, A., Thoulouze, M.I., Galli, T., Roux, P., Dautry-Varsat, A., and Alcover, A. (2004). Activation-induced polarized recycling targets T cell antigen receptors to the immunological synapse; involvement of SNARE complexes. Immunity *20*, 577–588.

Dustin, M.L. (2008). T-cell activation through immunological synapses and kinapses. Immunol. Rev. *221*, 77–89.

Dustin, M.L., Starr, T., Varma, R., and Thomas, V.K. (2007). Supported planar bilayers for study of the immunological synapse. Curr. Protoc. Immunol. *Chapter 18*, Unit 18.13.

Giurisato, E., Cella, M., Takai, T., Kurosaki, T., Feng, Y., Longmore, G.D., Colonna, M., and Shaw, A.S. (2007). Phosphatidylinositol 3-kinase activation is required to form the NKG2D immunological synapse. Mol. Cell. Biol. *27*, 8583–8599.

Grakoui, A., Bromley, S.K., Sumen, C., Davis, M.M., Shaw, A.S., Allen, P.M., and Dustin, M.L. (1999). The immunological synapse: A molecular machine controlling T cell activation. Science *285*, 221–227.

Huse, M., Lillemeier, B.F., Kuhns, M.S., Chen, D.S., and Davis, M.M. (2006). T cells use two directionally distinct pathways for cytokine secretion. Nat. Immunol. *7*, 247–255.

Kaizuka, Y., Douglass, A.D., Vardhana, S., Dustin, M.L., and Vale, R.D. (2009). The coreceptor CD2 uses plasma membrane microdomains to transduce signals in T cells. J. Cell Biol. *185*, 521–534.

Kay, A.R., Alfonso, A., Alford, S., Cline, H.T., Holgado, A.M., Sakmann, B., Snitsarev, V.A., Stricker, T.P., Takahashi, M., and Wu, L.G. (1999). Imaging synaptic activity in intact brain and slices with FM1–43 in C. elegans, lamprey, and rat. Neuron *24*, 809–817.

Lanier, L.L. (2005). NK cell recognition. Annu. Rev. Immunol. *23*, 225–274.

Liu, D., Xu, L., Yang, F., Li, D., Gong, F., and Xu, T. (2005). Rapid biogenesis and sensitization of secretory lysosomes in NK cells mediated by target-cell recognition. Proc. Natl. Acad. Sci. USA *102*, 123–127.

Monks, C.R., Freiberg, B.A., Kupfer, H., Sciaky, N., and Kupfer, A. (1998). Three-dimensional segregation of supramolecular activation clusters in T cells. Nature *395*, 82–86.

Moretta, A., Bottino, C., Vitale, M., Pende, D., Cantoni, C., Mingari, M.C., Biassoni, R., and Moretta, L. (2001). Activating receptors and coreceptors involved in human natural killer cell-mediated cytolysis. Annu. Rev. Immunol. *19*, 197–223.

Orange, J.S. (2008). Formation and function of the lytic NK-cell immunological synapse. Nat. Rev. Immunol. *8*, 713–725.

Orange, J.S., Harris, K.E., Andzelm, M.M., Valter, M.M., Geha, R.S., and Strominger, J.L. (2003). The mature activating natural killer cell immunologic synapse is formed in distinct stages. Proc. Natl. Acad. Sci. USA *100*, 14151–14156.

Roda-Navarro, P., Mittelbrunn, M., Ortega, M., Howie, D., Terhorst, C., Sanchez-Madrid, F., and Fernandez-Ruiz, E. (2004). Dynamic redistribution of the activating 2B4/SAP complex at the cytotoxic NK cell immune synapse. J. Immunol. *173*, 3640–3646.

Somersalo, K., Anikeeva, N., Sims, T.N., Thomas, V.K., Strong, R.K., Spies, T., Lebedeva, T., Sykulev, Y., and Dustin, M.L. (2004). Cytotoxic T lymphocytes form an antigen-independent ring junction. J. Clin. Invest. *113*, 49–57.

Stinchcombe, J.C., Bossi, G., Booth, S., and Griffiths, G.M. (2001). The immunological synapse of CTL contains a secretory domain and membrane bridges. Immunity *15*, 751–761.

Stinchcombe, J.C., and Griffiths, G.M. (2007). Secretory mechanisms in cell-mediated cytotoxicity. Annu. Rev. Cell Dev. Biol. *23*, 495–517.

Wulfing, C., Purtic, B., Klem, J., and Schatzle, J.D. (2003). Stepwise cytoskeletal polarization as a series of checkpoints in innate but not adaptive cytolytic killing. Proc. Natl. Acad. Sci. USA *100*, 7767–7772.

Yokosuka, T., Kobayashi, W., Sakata-Sogawa, K., Takamatsu, M., Hashimoto-Tane, A., Dustin, M.L., Tokunaga, M., and Saito, T. (2008). Spatiotemporal regulation of T cell costimulation by TCR-CD28 microclusters and protein kinase C theta translocation. Immunity *29*, 589–601.